



# Limits to resolution in composition and density in ultra high-pressure experiments on natural mantle-rock samples

Kanani K. M. Lee<sup>a,\*</sup>, Bridget O'Neill<sup>a,b</sup>, Raymond Jeanloz<sup>a</sup>

<sup>a</sup> Department of Earth and Planetary Science, University of California, Berkeley, 307 McCone Hall, Berkeley, CA 94720-4767, USA

<sup>b</sup> Lowell Observatory/NPOI, 1400 W. Mars Hill Road, Flagstaff, AZ 86001, USA

Received 24 February 2003; received in revised form 12 June 2003; accepted 24 June 2003

## Abstract

We compressed and analyzed an undepleted natural peridotite—thought to be representative of the Earth's upper mantle—from ~25 to 110 GPa and heated to 2000–2500 K. Scatter in zero-pressure unit-cell volumes observed for high-pressure phases synthesized from peridotite, of  $\pm 0.4\%$  for orthorhombic perovskite and  $\pm 0.8\%$  for magnesiowüstite, can be ascribed to compositional heterogeneity in the natural starting material and its transformation products (calcium perovskite was also observed at high pressures, but does not quench to zero pressure). The scatter is larger than the measurement uncertainties, which are as little as  $\pm 0.1\%$ , but is less than would be expected from the variation in composition among distinct minerals if the starting material had failed to equilibrate upon transformation to the high-pressure assemblage (e.g., up to  $\pm 0.6$ – $0.8\%$  in volume for orthorhombic perovskite). The equilibrium unit-cell volume of orthorhombic perovskite calculated from an average of electron microprobe analyses on the quenched samples,  $163.3 (\pm 0.6) \text{ \AA}^3$ , agrees to within 0.4% with the average value measured from the same samples by X-ray diffraction at zero pressure ( $163.9 \pm 0.7 \text{ \AA}^3$ ). Similarly, values of zero-pressure density for the whole-rock assemblage of high-pressure phases are identical ( $4.13 \pm 0.03 \text{ g/cm}^3$ ), whether derived from electron microprobe or X-ray diffraction measurements.

© 2004 Published by Elsevier B.V.

**Keywords:** Peridotite; Electron microscopy; Chemical analysis; High pressure; Diamond-anvil cells; X-ray diffraction analysis

## 1. Introduction

There is a great need for experiments that reproduce the conditions of high pressures and temperatures existing deep inside planets. In particular, it is important to characterize the properties of relevant materials at

deep-interior conditions in order to determine the constitution, state and evolution of the Earth and planets over geological time. Thus, it is only through high pressure-temperature studies that seismological and other geophysical observations can be interpreted in terms of the identities (e.g., crystal structures), abundances, compositions and other properties of the mineral phases of the Earth's deep interior. It is therefore important to quantify the reliability and resolution of the measurements obtained from high-pressure experiments so that one can determine the significance of models derived from the combined measurements and geophysical observations.

\* Corresponding author. Present address: Division of Geological and Planetary Sciences, California Institute of Technology, MC 170-25, Pasadena, CA 91125, USA. Tel.: +1-510-643-8325; fax: +1-510-643-9980.

E-mail addresses: [kanani@gps.caltech.edu](mailto:kanani@gps.caltech.edu) (K.K.M. Lee), [boneill@sextans.lowell.edu](mailto:boneill@sextans.lowell.edu) (B. O'Neill), [jeanloz@uclink.berkeley.edu](mailto:jeanloz@uclink.berkeley.edu) (R. Jeanloz).

The quality of such experiments is often described in terms of (i) the range and calibration of the pressures and temperatures that are achieved, and (ii) the quality of the measurements performed at high pressures. With the advent of the laser-heated diamond cell, it is now possible to reproduce essentially the full range of pressures and temperatures existing inside the Earth, and calibration of experimental conditions has received considerable attention to date (Jeanloz and Kavner, 1996; Knittle and Jeanloz, 1987; Mao et al., 1978; Shim et al., 2002). Similarly, the use of synchrotron- and laser-based probes, among other tools, has led to major advances in the quality of measurements that can be performed on samples at high pressures.

The role of the starting material has received relatively little attention, however, as a third source of uncertainty affecting the quality of high-pressure measurements. Indeed, the sample material is often chosen so as to minimize any possible degradation of the measurements. It is for this reason that most ultra-high-pressure ( $\sim 100$  GPa) studies to date have focused on the properties of single-phase and, in many cases, synthetic starting materials (e.g., Andraut, 2001; Fiquet et al., 1998; Knittle and Jeanloz, 1987). As the ultimate objective is to determine the properties of planetary materials at deep-interior conditions, however, it also becomes necessary to examine natural samples. This is so if for no other reason than to evaluate the effects of minor elements or the presence of minor (initial) phases on the final results. In addition, certain materials are intrinsically difficult to synthesize as truly homogeneous samples, with the most ideally uniform starting material being amorphous.

Ultramafic rocks, characteristic of the Earth's upper mantle and of chondritic meteorites, offer a good example of such difficulties. Bulk compositions corresponding to peridotite and similar rocks are refractory, and cannot be readily quenched to a glass from the melt. Even if a glass is formed on cooling (e.g., by splat quenching), melting temperatures are sufficiently high that moderately volatile elements such as Na and K are often lost during preparation of the starting sample. Sol-gel techniques can produce an amorphous and relatively uniform starting material of peridotite composition, but invariably lead to contamination, especially by hydrogen. Finally, mechanical comminution (e.g., by ball milling) can produce a uniform, fine-grained

and possibly amorphous sample, but with the potential of contamination from the grinding surfaces.

Consequently, it is difficult to obtain pure (uncontaminated) and uniform starting materials having the bulk composition of terrestrial mantles. Sample uniformity is especially critical for the highest-pressure experiments: these rely on small ( $\sim \mu\text{g}$ ) samples being compressed inside a diamond-anvil cell, in contrast with the larger ( $\sim \text{mg}$ ) samples that are compressed (but to lower peak pressures) in multi-anvil devices. For the latter, electron microprobe and other high-quality analytical tools can be used to confirm that individual mineral grains formed at high pressures have uniform and reproducible compositions. In comparison, it is much more difficult to document homogeneity—and therefore a close approach to equilibrium—for individual mineral phases produced in the laser-heated diamond cell.

The objective of the present work is to quantify the resolution in molar volume, composition and density of the high-pressure mineral-phase assemblage formed from a natural sample that is thought to have a bulk composition close to that of the Earth's mantle. In combination with seismological observations, these properties are important for modeling the constitution and state of the deep interior. Our focus here is on zero-pressure measurements, as these can reveal much about the reliability of the data: for example, beginning to quantify the degree to which the sample achieves (at least local) thermodynamic equilibrium, as well as the accuracy of such relevant properties as phase-composition and assemblage-density.

## **2. Lower-mantle assemblage formed from natural peridotite**

We address these issues, including the role of the initial sample in producing equilibrated high-pressure phases, by describing the high-pressure assemblage formed from a natural peridotite at lower-mantle pressures ( $\sim 25$ – $110$  GPa). This is but one example of the rock-types present in the earth's mantle, but is of special interest because it is thought to correspond to the bulk composition of at least the upper mantle (e.g., Ringwood, 1975). The starting material (BN-35), with bulk composition and mineral constituents given in Table 1 (Stern et al., 1986), was transformed in two

Table 1  
Composition of BN-35 and its individual phases in wt.% (Stern et al., 1986)

	BN-35 whole-rock composition <sup>a</sup>	Olivine 45 vol.% 43 mol%	Orthopyroxene 25 vol.% 33 mol%	Clinopyroxene 15 vol.% 19 mol%	Garnet 15 vol.% 5 mol%
SiO <sub>2</sub>	45.40 (0.26)	34.08	56.89	53.31	43.94
TiO <sub>2</sub>	0.25 (0.06)	0.29	0.10	0.45	0.16
Al <sub>2</sub> O <sub>3</sub>	4.30 (0.69)	4.02	3.49	5.73	23.19
Cr <sub>2</sub> O <sub>3</sub>	0.30 (0.02)	0	0.35	0.83	1.16
FeO <sup>b</sup>	8.30 (0.53)	10.97	7.63	3.13	8.06
MnO	0.14 (0.01)	0.24	0.08	0.04	0.24
MgO	37.10 (0.93)	52.57	30.99	15.43	19.88
CaO	3.30 (0.13)	0	0.76	20.11	4.97
Na <sub>2</sub> O	0.30 (0.03)	0.19	–	1.37	–
K <sub>2</sub> O	0.0 (–)	–	–	–	–
NiO	0.24 (–)	–	–	–	–
Total	99.63	102.36	100.29	100.4	101.6
$x_{\text{Fe}} = \text{Fe}/(\text{Fe}+\text{Mg})$	0.11 (0.02)	0.10	0.12	0.10	0.19
$\text{Mg\#} = \text{Mg}/(\text{Mg}+\text{Fe})$	0.89 (0.02)	0.90	0.88	0.90	0.81

<sup>a</sup> Uncertainties are given in parentheses and are determined by taking the difference in element abundances from an independent measurement of the starting sample (O'Neill, 1994).

<sup>b</sup> Fe<sup>2+</sup> and Fe<sup>3+</sup> totals are combined.

sets of experiments using laser-heated diamond cells (diamond culet size ranging from 100 to 350  $\mu\text{m}$ ) using pre-compressed (to  $\sim 20$ – $40 \mu\text{m}$  thick) Re or Fe gaskets. In all cases, pressures were determined before and after laser heating using the ruby-fluorescence scale (Mao et al., 1978), with only the values after heating being quoted here. In both sets of experiments, the sample was laser heated by rastering it under the focused beam (hot-spot diameter  $\sim 20 \mu\text{m}$ ) of a continuous (cw) TEM<sub>00</sub>-mode Nd-YAG ( $\lambda = 1064 \text{ nm}$ ) laser, keeping clear of the very edges of the gasket and ruby calibrant to minimize the possibility of contamination. Heating duration at any one spot was short (seconds) at any particular time, in order to minimize the Soret diffusion of Fe out of the hot spot, with total heating of the entire sample taking approximately 10–30 min (both for synthesis and annealing). The laser power was kept sufficiently low to avoid melting, and we observed no evidence of melting either during heating or through analysis of the sample after heating.

Of the two sets of experiments, each run in the first set consisted of compressing a fresh sample of peridotite to a given pressure, laser-heating the sample to temperatures of 2000–2500 K, and then obtaining X-ray diffraction patterns at room temperature before and after decompressing the

sample to zero pressure (O'Neill, 1994; O'Neill and Jeanloz, 1990). All of these diffraction patterns were collected at room temperature, using monochromatic Mo K $\alpha$  ( $\lambda = 0.7107 \text{ \AA}$ ) radiation from a rotating-anode source at high pressures and filtered Cu K $\alpha$  ( $\lambda = 1.5418 \text{ \AA}$ ) radiation from a standard tube at zero pressure (after the sample was removed from the diamond cell). In both the cases, the beam size was comparable to the diameter of the sample,  $\sim 100$ – $150 \mu\text{m}$ . The diffraction patterns were collected on film that was digitized and analyzed as described elsewhere (Nguyen and Jeanloz, 1993), and with fitting of individual peaks to determine constituent phase unit-cell volumes (O'Neill, 1994).

In the second set of experiments, the sample was loaded in an Ar medium and laser heated to 2000–2500 K at pressures of 30–52 GPa in order to convert the peridotite to the high-pressure assemblage. X-ray diffraction patterns were then collected at several pressures, on compression to peak pressures of 47–87 GPa and decompression to zero pressure (sample outside the diamond cell), with laser-heating used to further anneal the samples at 41, 47, 66, 78 and 87 GPa. All of the diffraction patterns for the second set of experiments were collected at room temperature using synchrotron radiation and image plates, with the size of the X-ray beam ranging from

60  $\mu\text{m}$  (i.e., much smaller than the sample) for the high-pressure runs to more than 100  $\mu\text{m}$  diameter upon quench (Fig. 1A and B). Data were collected at Stanford Synchrotron Radiation Laboratory (SSRL) beamline 10-2 and Advanced Photon Source (APS) beamline 13-IDD, and were analyzed both through individual fitting of peaks (as in the first set of experiments) and by Rietveld analysis (Larson and Von Dreele, 2000; Toby, 2001) (Fig. 1B).

In both sets of experiments, the samples transformed to assemblages of 64 ( $\pm 2$ ) mol% (Mg, Fe, Al)SiO<sub>3</sub> orthorhombic perovskite (opv), 31 ( $\pm 2$ ) mol% (Mg, Fe)O magnesiowüstite (mw) and 5 ( $\pm 1$ )

mol% CaSiO<sub>3</sub> perovskite (cpv), where the relative proportions were determined from the bulk composition of the starting material (see Table 1) and the compositions of the high-pressure mineral phases deduced from the lattice parameters obtained from the X-ray patterns (Jeanloz and Thompson, 1983; O'Neill, 1994; O'Neill and Jeanloz, 1990). These results are compatible with the mineral-phase proportions obtained in the Rietveld fits, so can be considered independently verified.

Complete and essentially smooth powder-diffraction lines were obtained, with some amount of spottiness (from grain growth upon transformation) observed in

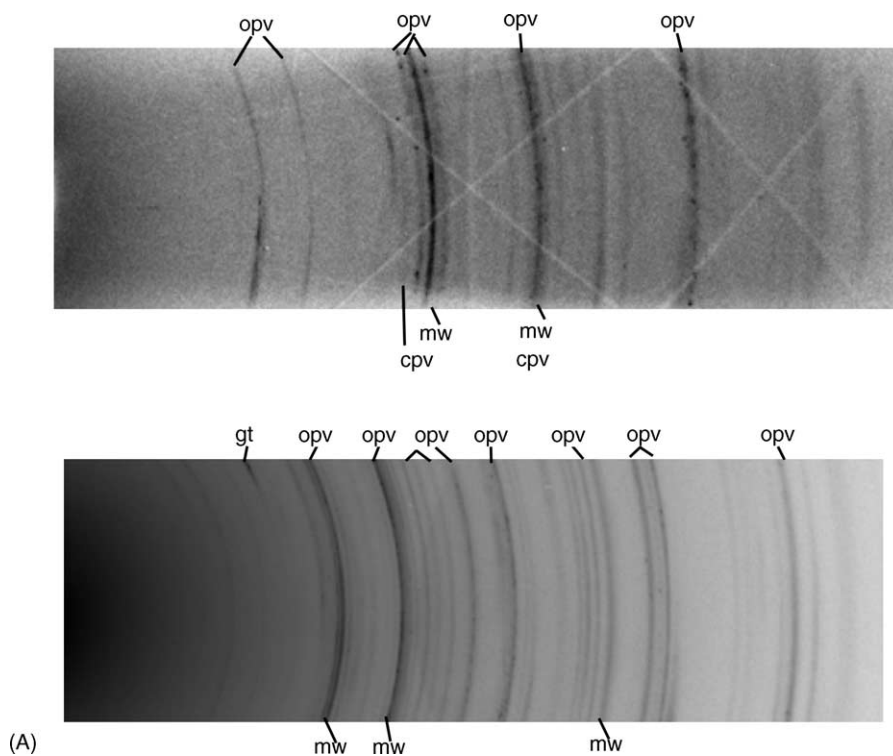


Fig. 1. (A) X-ray diffraction patterns of sample Per\_500 at a pressure of 51.8 ( $\pm 0.5$ ) GPa (top) and at zero pressure (bottom), taken after laser heating and conversion to the high-pressure mineral assemblage. The main diffraction lines of the high-pressure phases are labeled: orthorhombic perovskite (opv), magnesiowüstite (mw) and calcium perovskite (cpv). The data were collected at room temperature at SSRL, using monochromatic radiation ( $\lambda = 0.7277 \text{ \AA}$ ) and image plates. The high-pressure diffraction pattern was obtained using a 60  $\mu\text{m}$  diameter X-ray beam, and the zero-pressure pattern was obtained using a 150  $\mu\text{m}$  diameter beam. Only half the diffraction pattern is shown in each case, and the cross-cutting diagonal lines in the upper pattern are ascribed to Kossel fringes (Lang, 1998) from the diamond anvil (the pattern at zero pressure is of only the sample, without the diamonds). (B) Rietveld refined X-ray diffraction patterns at 51.8 ( $\pm 0.5$ ) GPa (top) and quenched (bottom) shown in A. Dots are the actual data while the line is the calculated Rietveld fit. Phase diffraction-line positions shown as ticks below each pattern, in descending order: orthorhombic perovskite, magnesiowüstite, and calcium perovskite (or garnet (gt) in quenched pattern). Garnet is seen only in the quenched patterns (and only at the  $\sim 0.1$  wt.% level) as the X-ray beam probes a larger portion of the sample, including the edges that were not heated and are thus unconverted.

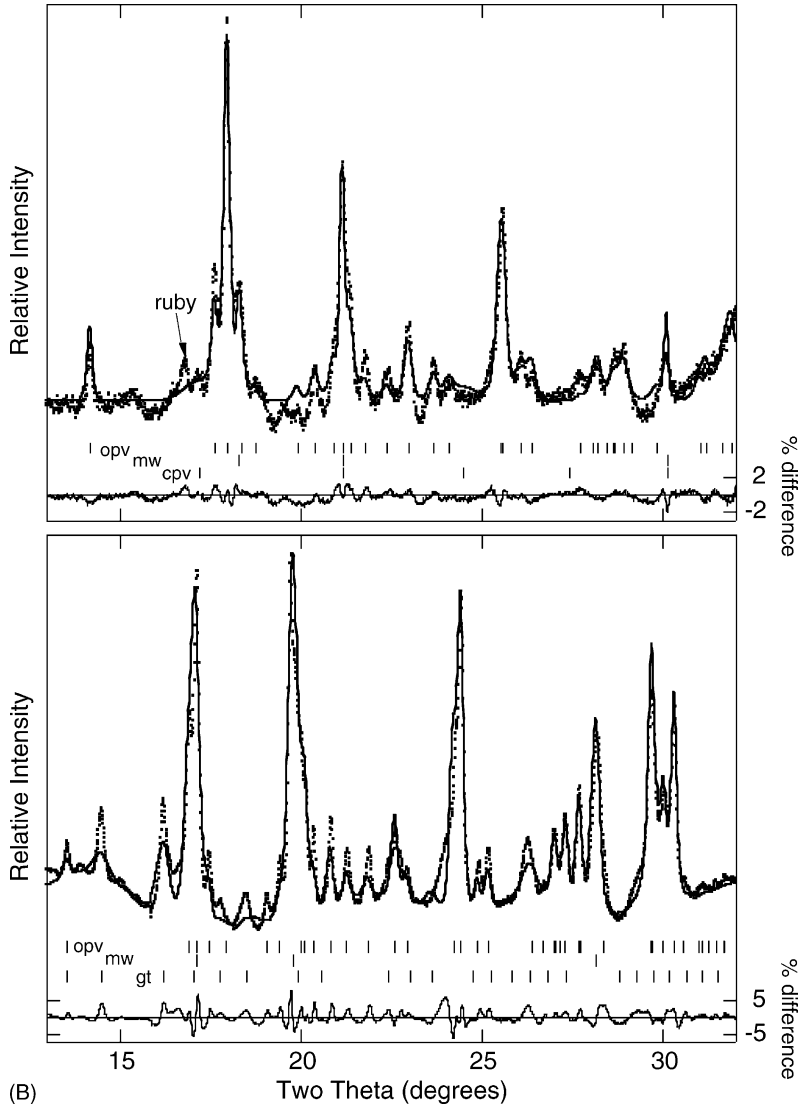


Fig. 1. (Continued).

patterns taken with higher spatial resolution (Fig. 1A). The character of the diffraction rings is in line with observations by optical microscopy, which indicate the presence of occasional crystals as large as 2–5  $\mu\text{m}$  but the bulk of the transformed sample having crystal sizes under 1–2  $\mu\text{m}$ . The important point is that the individual crystals were much smaller than the laser-heated spot, both before and after transformation.

Overall, the quality of the diffraction patterns indicates good conversion to the high-pressure assem-

blage. Except for minor amounts of garnet remaining after heating at pressures below 30–35 GPa, none of the starting material was evident in the diffraction patterns from the heated portions of each sample. Of course, starting material was present in the unheated portions of the samples (e.g., next to the gasket), as we were able to distinguish by comparing diffraction patterns obtained using a small-diameter X-ray beam taken at high pressures with large-diameter beam patterns taken at zero pressure (Fig. 1). The presence of

garnet in the heated portions of the lowest-pressure runs is consistent with phase equilibria determined in independent studies (e.g., Kubo and Akaogi, 2000) and with other methods, so does not indicate an inability to transform the entire sample or any other indication of deviation from phase-equilibrium. Because of the small amount of calcium perovskite present in the high-pressure assemblage, and the fact that it becomes

amorphous (so has no diffraction lines) on quenching to zero pressure, we limit our present discussion of the diffraction patterns to results for orthorhombic perovskite and magnesiowüstite.

The quality of data obtained from the natural peridotite starting material is quantified in Fig. 2, which shows the scatter in unit-cell volumes for orthorhombic perovskite and magnesiowüstite being about  $\pm 1\%$

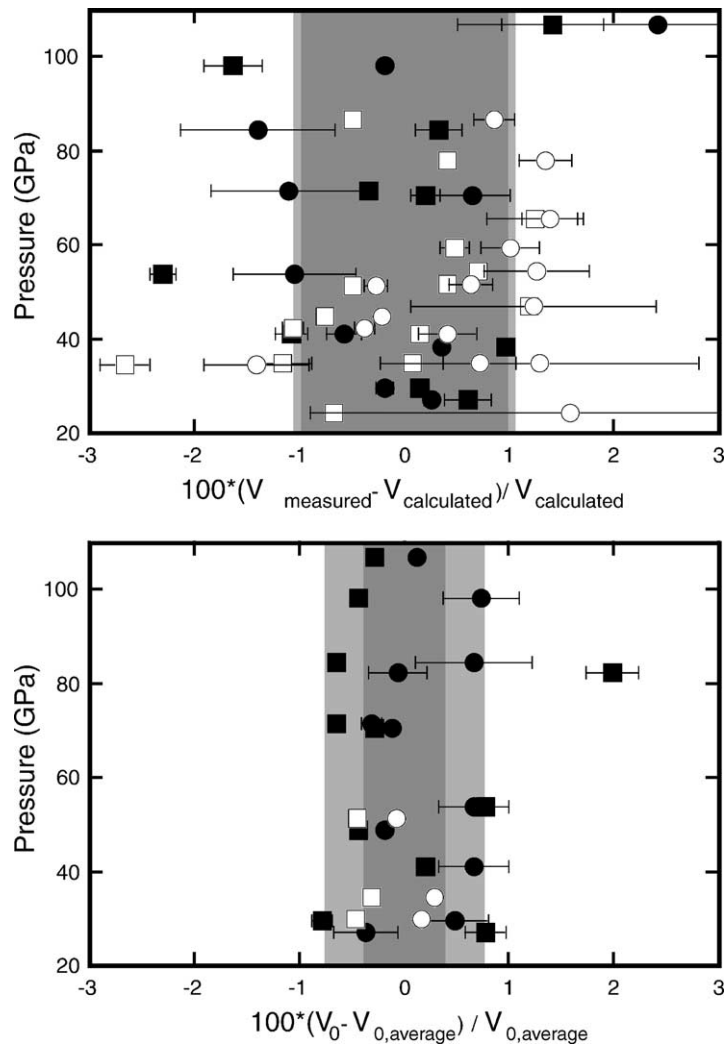


Fig. 2. Percent deviation in unit-cell volumes ( $V$ ) for orthorhombic perovskite (circles) and magnesiowüstite (squares), shown as a function of pressure at high pressure (top) and as a function of synthesis pressure at zero pressure (bottom). Open and closed symbols designate samples loaded with and without an Ar pressure medium, respectively, and error bars indicate measurement uncertainties when these exceed the size of the symbol. Deviations are calculated from our measured equations of state at high pressures (Lee et al., 2003; O'Neill, 1994), and from weighted-mean values of  $163.90 (\pm 0.67) \text{ \AA}^3$  for opv and  $76.09 (\pm 0.60) \text{ \AA}^3$  for mw at zero pressure. Standard deviations reflecting the observed scatter are shown by dark shading for orthorhombic perovskite and light shading for magnesiowüstite.

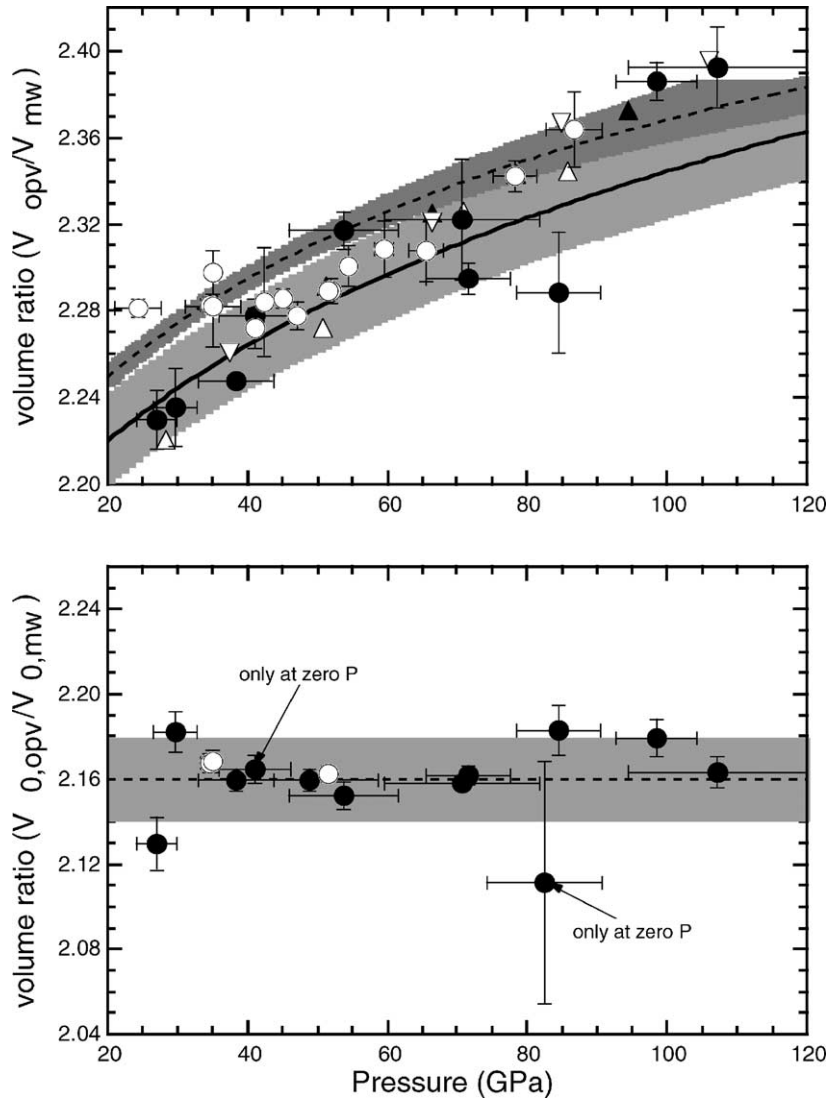


Fig. 3. Volume ratio of orthorhombic perovskite to magnesiowüstite  $V_{\text{opv}}/V_{\text{mw}}$  as a function of pressure at high pressure (top) and as a function of synthesis pressure at zero pressure (bottom). Top: circles are our data, with argon as a pressure medium (open circles) and without argon (closed circles). To compare we also plot data from Table 2 from Andraut's (2001) high-pressure study of San Carlos olivine (open triangles), alumina + San Carlos olivine (closed triangles) and a San Carlos olivine equilibrated at oxygen fugacity  $f_{\text{O}_2}$  of  $8.6 \times 10^{-10}$  atm (inverted open triangles). The dashed curve shows the predicted volume ratio for pure Mg endmembers,  $V_{\text{MgSiO}_3}/V_{\text{MgO}}$  (dark band indicates uncertainties), whereas the solid curve shows the volume ratio as a function of pressure derived from our equations of state and assuming no effect of pressure on the Mg/Fe distribution ratio between opv and mw (light band indicates uncertainties; at the highest pressures uncertainties are overlaid by the uncertainties of the pure Mg endmembers (dark band)). Bottom: at zero pressure, the average value observed for  $V_{0,\text{opv}}/V_{0,\text{mw}}$  is  $2.16 (\pm 0.02)$  (dashed line with shaded band indicating uncertainty), and the individual values show no trends with synthesis pressure. Samples for which measurements were only taken at zero pressure (after synthesis at high pressure) are marked. Error bars indicate measurement uncertainties.

at high pressures and  $\pm 0.4$ – $0.8\%$  upon quenching to zero pressure (average values, indicated by shading in the figure, are quoted here). Uncertainties in the volumes (individual error bars) range from less than  $\pm 0.1\%$  to as much as  $\pm 1.0$ – $2.5\%$ , and are generally much less than the scatter.

Both the uncertainties and scatter are larger by  $\sim 25$ – $65\%$  at high pressures than upon quenching. This is partly due to some of the high-pressure patterns being of lower quality than the zero-pressure data, mainly because of the effects of diamond absorption (because the zero-pressure patterns were obtained from samples outside the diamond cell). Additionally, overlapping diffraction lines and uncertainties in the sample pressure also contribute to the increased scatter between observed and calculated volumes at high pressures. In particular, measured variations in pressure across a sample were as small as  $0.2$  GPa and as large as  $12.6$  GPa, which corresponds to volume uncertainties of  $\pm 0.2$ – $5.0\%$  (calculated using a Birch–Murnaghan equation of state (Birch, 1978)). Non-hydrostaticity may further degrade some of the high-pressure measurements, although we have found no correlation between the measured pressure variations across samples (or the presence or absence of an Ar medium) and the observed scatter.

Following Andrault (2001), we look at the volume ratio between opv and mw,  $V_{\text{opv}}/V_{\text{mw}}$  (Fig. 3). At zero pressure we find an average  $V_{0,\text{opv}}/V_{0,\text{mw}}$  of  $2.16$  ( $\pm 0.02$ ) without any noticeable dependence on synthesis pressure, and the results in Fig. 3 (bottom) are merely another representation of the data shown in Fig. 2 (bottom). Following early partitioning experiments (Bell et al., 1979; Yagi et al., 1979), this would suggest that the Mg/Fe distribution coefficient between opv and mw does not depend on pressure, and is otherwise not affected by synthesis conditions over the range covered in the present study.

At high pressure,  $V_{\text{opv}}/V_{\text{mw}}$  is not constant due to the differences in the compressibilities of opv and mw. As Andrault points out (Andrault, 2001), any deviations from the predicted Mg-endmember volume ratio (dashed curve and dark shading in Fig. 3, top) may be attributable to a change in partitioning behavior with pressure. His analysis, however, does not include any effects of Al upon the equation of state of opv nor the uncertainties in the respective equations of state. When we do take these factors into account, we find

that within the uncertainties of the known equations of state (solid curve and light shading in Fig. 3, top (Lee et al., 2003)) we cannot confirm any changes of partitioning with pressure. Additionally, the measurements collected at zero pressure appear to rule out such a pressure dependence, at least within our uncertainties. For the Mg-endmembers, we use the Birch–Murnaghan equation of state with the following values for the parameters  $V_0$ ,  $K_{0T}$  and  $K'_{0T}$ : MgSiO<sub>3</sub>  $162.47$  ( $\pm 0.31$ )  $\text{\AA}^3$ ,  $263$  ( $\pm 3$ ) GPa,  $3.9$  ( $\pm 0.5$ ); MgO  $74.7243$  ( $\pm 0.0537$ )  $\text{\AA}^3$ ,  $162.7$  ( $\pm 2.9$ ) GPa,  $4.1$  ( $\pm 0.1$ ) (Andrault, 2001; Jeanloz and Hemley, 1994; Jeanloz and Thompson, 1983).

The high-pressure measurements are therefore compatible with what we infer from the zero-pressure volumes (Fig. 2, bottom) or volume ratios (Fig. 3, bottom), namely that there is no evidence for a shift in Mg/Fe partitioning between opv and mw between  $25$  and  $110$  GPa. This is in contrast with inferences recently derived from high-pressure X-ray spectroscopy on magnesiowüstite (Badro et al., 2003) that suggest an increase of several orders of magnitude in the Fe partitioning between magnesiowüstite and orthorhombic perovskite, perhaps because we are studying a more complex (i.e., natural, Al-bearing) bulk composition in the present experiment. The remaining scatter, of  $\pm 0.4$  and  $\pm 0.8\%$  observed for the volumes of opv and mw at zero pressure, can be ascribed to compositional variations in the high-pressure mineral phases.

Overall, as much as  $1/2$ – $2/3$  of the uncertainty in the opv and mw volumes measured at high pressures is of the same magnitude as—so can be ascribed to the same factors causing—the scatter in volumes observed at zero pressure (Figs. 2 and 3). If there is a systematic correlation between volume deviations for a given sample at high pressures and at zero pressure, however (e.g., Fig. 2, top and bottom), any such correlation is obscured by the added uncertainties in the high-pressure measurements. Consequently, we now focus on the scatter in opv and mw unit-cell volumes measured at zero pressure, and note that it exhibits no correlation with synthesis pressure (Figs. 2 and 3).

### 3. Electron microprobe analyses

In order to determine whether or not the observed scatter in unit-cell volumes is due to variations in

composition, we have performed electron microprobe analyses on several of the quenched samples. The conditions of synthesis, high pressures and temperatures achieved between smooth diamond culet faces, ensure that the transformed peridotite often has a smooth surface suitable for microprobe analysis (Fig. 4). Samples still encased in their gaskets were mounted on glass slides, cleaned and carbon coated. A Cameca SX-51 electron microprobe was used with a 15 keV electron

beam focused to a spot size  $\leq 5 \mu\text{m}$  diameter at the sample, and pure metal oxides served as standards (Pingitore et al., 1999).

Abundances were determined for Si, Ti, Al, Fe, Mg, Ca, Na and K. Because oxygen was not included in the analyses, the data were reduced assuming stoichiometric compositions. Earlier analyses (Knittle and Jeanloz, 1991), which did include oxygen, provide support for orthorhombic perovskite having

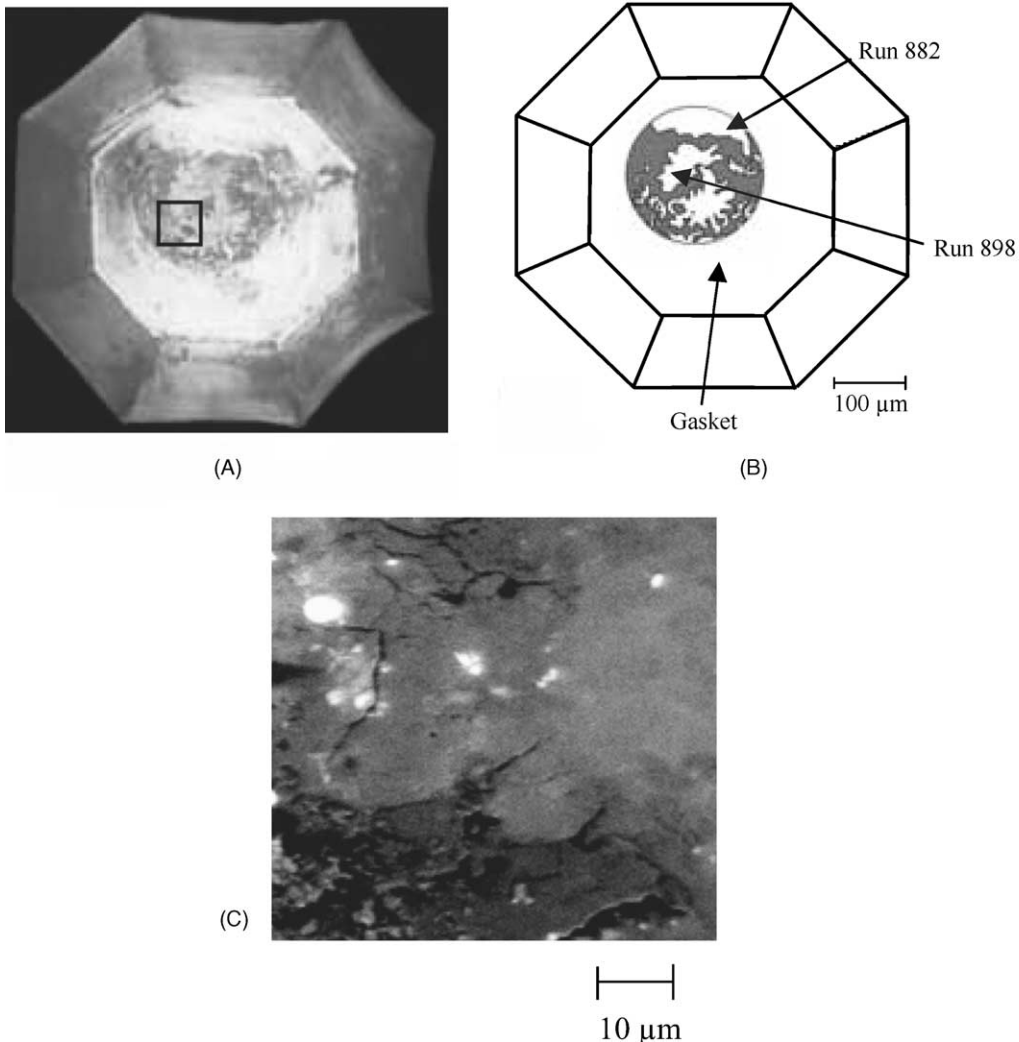


Fig. 4. (A) Photomicrograph in both reflected and transmitted light, and (B) schematic drawing of sample Per\_500 quenched to zero pressure after heating, initially at 35 GPa, and compression up to 65 GPa. The locations of microprobe analyses 882 and 898 are marked for reference, and the bright area around the sample is gasket material. Scale bar is 100  $\mu\text{m}$ . (C) Back-scattered electron image (mw appears as bright spots) of region of Per\_500 shown in box in A, obtained with an electron beam at 10.00 keV and current of 600 pA. Scale bar is 10  $\mu\text{m}$ . The variations in gray—hence, variations in mean atomic number—in the matrix show the sample's heterogeneity.

Table 2  
Electron microprobe analyses of quenched samples in wt.%

Sample analysis	Per_500		Per_601		Average (nine analyses)
	882	898	911	919	
SiO <sub>2</sub>	52.34	51.53	44.42	39.98	45.89 (6.32)
TiO <sub>2</sub>	0.17	0.12	0.14	0.00	0.08 (0.07)
Al <sub>2</sub> O <sub>3</sub>	3.87	7.56	1.62	0.20	2.96 (2.94)
FeO	6.47	5.90	9.41	10.19	8.20 (1.96)
MgO	36.32	32.08	43.19	48.86	41.74 (7.57)
CaO	0.74	0.93	1.23	0.14	0.66 (0.37)
Na <sub>2</sub> O	0.17	0.13	0.15	0.02	0.11 (0.06)
K <sub>2</sub> O	0.02	0.02	0.04	0.01	0.01 (0.01)
Sum	100.10	98.26	100.18	99.39	99.65 (0.81)

stoichiometric composition when formed in the laser-heated diamond cell at comparable pressures and temperatures. However, we note that there is considerable interest in the possibilities of nonstoichiometry and of point defects in opv; this is especially so for more complex (e.g., Al-bearing) compositions, such as may be relevant to the present study (e.g., Navrotsky et al., 2002). Low totals were obtained in some analyses, however these can all be attributed to poor surface conditions or sample orientation in the present experiments. Only those analyses with totals between 98.0 and 102.0% are discussed here (almost all the rejected analyses came from one sample with a poor surface).

Although typical sample dimensions exceed 100  $\mu\text{m}$  in diameter (Fig. 4), an average of only nine analyses is already in good agreement (within mutual uncertainties) with the bulk composition of the rock, except for a deficiency in CaO (Table 2). Because of the fine (mostly sub- $\mu\text{m}$ ) grain size of the transformed sample, each analysis is an average over a mixture of the three high-pressure phases, opv, mw and cpv. Indeed, it is impossible to interpret the analyses as being an average over fewer than 2–3 of the high-pressure mineral phases (e.g., an Mg/Si ratio exceeding 1 may be inferred for opv). Four individual analyses illustrating the range of observed compositions are listed in Table 2, and confirm that there can be quite a bit of variability from one spot to another within a sample, as well as from sample to sample.

Interpreting the scatter in individual analyses as being due to varying amounts of opv, mw, cpv and ruby (contamination from the pressure calibrant), we are able to estimate the composition of opv (and rela-

tive abundances of each phase) based on two assumptions. First, we assume that  $x_{\text{Fe}} = 0.20$  for mw, based on the zero pressure lattice-parameter determined by X-ray diffraction (Jeanloz and Thompson, 1983). Second, we assume that cpv is pure CaSiO<sub>3</sub>, based on the high-pressure volumes being compatible with those previously measured for pure cpv (O'Neill, 1994). Also, there is so little cpv in the high-pressure assemblage that even if the maximum amount of Al that has been observed to enter the structure is assigned to this phase (Takafuji et al., 2002), our conclusions are unaffected within quoted uncertainties. We then calculate the unit-cell volumes for the inferred composition of opv, taking into account aluminum as well as iron substitution (O'Neill and Jeanloz, 1994).

Our calculated opv zero-pressure volumes for the average of nine analyses ( $V_0 = 163.3 \pm 0.6 \text{ \AA}^3$ ) are in excellent agreement with the observed average opv volume ( $V_0 = 163.9 \pm 0.7 \text{ \AA}^3$ ) for those same samples (Table 3). The opv volumes inferred from the individual microprobe analyses generally overlap the values observed for the same samples (e.g., Per\_500), but not always Per\_601). The difference of up to 0.7% among individual calculated volumes is larger than the estimated uncertainties ( $\pm 0.1$ – $0.2\%$ ), but the average of calculated volumes is still within the uncertainty for the volumes observed by X-ray diffraction ( $\pm 0.4\%$ ). A similar conclusion is reached for the calculated densities of opv, which exhibit differences as large as 4.4% for the individual analyses but an uncertainty less than  $\pm 1.5\%$  for the average (Table 3).

These results confirm that the observed scatter in X-ray diffraction measurements at zero pressure can

Table 3

Orthorhombic perovskite compositions inferred from electron microprobe analyses (per 3 O)<sup>a</sup>

Sample analysis	Per_500		Per_601		Average (nine analyses)
	882	898	911	919	
Mg	0.88 ± 0.03	0.87 ± 0.02	0.88 ± 0.07	1.00 ± 0.03	0.93 ± 0.08
Fe	0.07 ± 0.01	0.09 ± 0	0.17 ± 0.02	0 ± 0.02	0.06 ± 0.06
Al	0.08 ± 0.01	0.12 ± 0.04	0.04 ± 0	0.01 ± 0	0.06 ± 0.05
Si	0.97 ± 0.03	0.92 ± 0.02	0.91 ± 0.09	0.99 ± 0.01	0.95 ± 0.05
Calculated opv $V_0$ (Å <sup>3</sup> )	163.43 ± 0.17	163.76 ± 0.21	163.80 ± 0.23	162.64 ± 0.17	163.26 ± 0.62
Observed opv $V_0$ (Å <sup>3</sup> )	164.37 ± 0.19		164.17 ± 0.32		163.90 ± 0.67
Calculated opv $\rho_0$ (g/cm <sup>3</sup> )	4.17 ± 0.02	4.19 ± 0.02	4.29 ± 0.02	4.10 ± 0.04	4.16 ± 0.06

<sup>a</sup> Assumes that the magnesiowüstite is of composition (Mg<sub>0.80</sub>Fe<sub>0.20</sub>)O; all of the Ca is in a pure CaSiO<sub>3</sub>; and that there might be a finite amount of ruby contamination. Using the volume relation of orthorhombic perovskite with Fe and Al, we calculate the zero-pressure unit-cell volume ( $V_0$ ) and density ( $\rho_0$ ) based on the composition determined by electron microprobe analysis (O'Neill and Jeanloz, 1994). Values indicated as '0' mean less than 0.5%.

be completely explained in terms of compositional heterogeneity in the high-pressure assemblage formed from a natural rock sample. Indeed, the X-ray data represent more nearly the average composition of the sample, in comparison with the individual electron microprobe analyses that reflect more of the local heterogeneity within each sample. This is not surprising, given the different sampling volumes characterizing the two methods in the present study: ~5 and ~60  $\mu\text{m}$  diameter for the microprobe and diffraction analyses, respectively.

#### 4. Discussion and conclusions

In order to quantify the range of compositional heterogeneity that might be expected in our samples, we consider the possibility that the individual minerals of the starting material each transforms to the high-pressure phases but without equilibrating amongst each other. Based on the composition and mode of BN-35 (Table 1), we find that the fractional molar abundances of iron and aluminum in the orthorhombic perovskite can vary over the range  $x_{\text{Fe}} = 0.10\text{--}0.20$  and  $x_{\text{Al}} (= \text{Al}/(\text{Al} + \text{Mg})) = 0.06\text{--}0.48$  (Table 4). Similarly, the molar abundance of iron in magnesiowüstite is in the range  $x_{\text{Fe}} = 0.00\text{--}0.10$  (mw is derived only from the initial olivine, in this instance).

This calculated variability in composition is larger than we observe, as is the corresponding scatter in calculated zero-pressure volumes: e.g., up to 1.2–1.6%

expected volume differences (i.e., up to  $\pm 0.6\text{--}0.8\%$  scatter) for opv (see Table 4), as compared with  $\pm 0.4\%$  observed (Fig. 2, bottom). Therefore, we conclude that whereas compositional variation across the entire sample is reflected in the observed variability in zero-pressure volumes (and electron microprobe analyses), there is at least an approach to equilibration between the high-pressure mineral phases formed from the distinct minerals in the starting material. That is, equilibrium is sufficiently well achieved to yield a reproducible assemblage of phases having relatively well-defined compositions and unit-cell volumes.

The variability in bulk starting composition (Table 1) can explain the scatter in the observed properties of the quenched samples (Figs. 2 and 3). The resulting uncertainty in properties at zero pressure is then generally convolved with additional uncertainties for in-situ measurements at high pressures. In the present case, the average observed uncertainty in unit-cell volumes is roughly 50% greater at high pressures than at zero pressure.

Nevertheless, covariation among the properties of the individual mineral phases can lead to relatively well-constrained properties for the whole-rock assemblage. For example, the whole-rock, zero-pressure densities calculated from analyses 911 and 919 of Tables 2 and 3 are 4.11 and 4.15 g/cm<sup>3</sup>, respectively, a difference of only 1% (as opposed to the nearly 5% difference in opv densities given in Table 3). For comparison, the whole-rock density calculated for the average of nine microprobe analyses is 4.13 ( $\pm 0.03$ ) g/cm<sup>3</sup>, and is identical to the density

Table 4

Decomposition reactions of initial minerals to lower-mantle phases<sup>a</sup>

Reaction	Starting composition <sup>b</sup>	Orthorhombic perovskite composition	Magnesiowüstite or calcium perovskite composition
Olivine → orthorhombic perovskite + magnesiowüstite Calculated $V_0$ ( $\text{\AA}^3$ ) <sup>c,d</sup>	(Mg <sub>1.90</sub> , Fe <sub>0.22</sub> , Al <sub>0.06</sub> , Si <sub>0.82</sub> )O <sub>4</sub>	(Mg <sub>1.00–0.90</sub> , Fe <sub>0.12–0.22</sub> , Al <sub>0.06</sub> , Si <sub>0.82</sub> )O <sub>3</sub>	(Mg <sub>0.90–1.00</sub> , Fe <sub>0.10–0.00</sub> )O
Orthopyroxene → orthorhombic perovskite + calcium perovskite Calculated $V_0$ ( $\text{\AA}^3$ ) <sup>c</sup>	(Mg <sub>0.81</sub> , Fe <sub>0.11</sub> , Al <sub>0.07</sub> , Ca <sub>0.01</sub> ) SiO <sub>3</sub>	(Mg <sub>0.82</sub> , Fe <sub>0.11</sub> , Al <sub>0.07</sub> ) SiO <sub>3</sub>	CaSiO <sub>3</sub>
Clinopyroxene → orthorhombic perovskite + calcium perovskite Calculated $V_0$ ( $\text{\AA}^3$ ) <sup>c</sup>	(Ca <sub>0.40</sub> , Mg <sub>0.43</sub> , Fe <sub>0.05</sub> , Al <sub>0.13</sub> , Si <sub>0.99</sub> )O <sub>3</sub>	(Mg <sub>0.72</sub> , Fe <sub>0.08</sub> , Al <sub>0.22</sub> , Si <sub>0.98</sub> )O <sub>3</sub>	CaSiO <sub>3</sub>
Garnet → orthorhombic perovskite + calcium perovskite Calculated $V_0$ ( $\text{\AA}^3$ ) <sup>c</sup>	(Mg <sub>2.10</sub> , Fe <sub>0.48</sub> , Ca <sub>0.37</sub> , Al <sub>1.94</sub> , Si <sub>3.11</sub> )O <sub>12</sub>	(Mg <sub>0.58</sub> , Fe <sub>0.13</sub> , Al <sub>0.53</sub> , Si <sub>0.76</sub> )O <sub>3</sub>	CaSiO <sub>3</sub>

<sup>a</sup> Based on a mass balance, allowing some defects or nonstoichiometry (corresponding to up to  $-6.3$  to  $+2.0\%$  deviation from charge balance).

<sup>b</sup> Whole-rock and individual phase compositions from Table 1 (Stern et al., 1986).

<sup>c</sup>  $V_0$  calculated for orthorhombic perovskite from (O'Neill and Jeanloz, 1994).

<sup>d</sup>  $V_0$  calculated for magnesiowüstite from (Jeanloz and Thompson, 1983).

determined entirely from the X-ray diffraction measurements ( $4.13 \pm 0.02$  g/cm<sup>3</sup>).

The reason for this good agreement is that the bulk composition of the rock already determines the mean atomic weight of the sample, so that the density is really determined to within the resolution of the average volumes of the mineral phases. Thus, the zero-pressure density of the assemblage can be obtained by two methods, purely from the X-ray diffraction data (calculated phase compositions and abundances) or purely from the electron microprobe analyses (calculated phase volumes and compositions), and the results agree to well within the  $\pm 0.5\%$  uncertainty of either approach. This agreement is important for geophysical applications because it means that the results of high-pressure experiments can be used to quantitatively interpret seismologically observed values of density and elastic moduli for the Earth's deep mantle.

## Acknowledgements

We thank M. Feineman for her expertise in and help with collection of the electron microprobe data. We also thank W.R. Panero and L.R. Benedetti for their experimental assistance, E. Girdt for artwork help

and S.-H. Shim, L.C. Ming and S.M. Clark for helpful discussions. We thank two anonymous reviewers for a thorough inspection of the manuscript that enabled us to better clarify our presentation. This research was supported by the US National Science Foundation. Portions of this research were carried out at the Stanford Synchrotron Radiation Laboratory, a national user facility operated by Stanford University on behalf of the US Department of Energy, Office of Basic Energy Sciences. Use of the Advanced Photon Source was supported by the US Department of Energy, Office of Basic Energy Sciences, under Contract No. W-31-109-Eng-38.

## References

- Andraut, D., 2001. Evaluation of (Mg, Fe) partitioning between silicate perovskite and magnesiowüstite up to 120 GPa and 2300 K. *J. Geophys. Res.* 106 (B2), 2079–2087.
- Badro, J., et al., 2003. Iron partitioning in Earth's mantle: toward a deep lower mantle discontinuity. *Science* 300 (5620), 789–791.
- Bell, P.M., Yagi, T., Mao, H.K., 1979. Iron-magnesium distribution coefficients between spinel [(Mg, Fe)<sub>2</sub>SiO<sub>4</sub>], Magnesiowüstite [(Mg, Fe)O], and Perovskite [(Mg, Fe)SiO<sub>3</sub>]. *Carnegie Inst. Washington Year Book* 78 (1790), 618–621.
- Birch, F., 1978. Finite strain isotherm and velocities for single-crystal and polycrystalline NaCl at high pressures and 300 K. *J. Geophys. Res.* 83, 1258–1267.

- Fiquet, G., et al., 1998. P-V-T equation of state of  $\text{MgSiO}_3$  perovskite. *Phys. Earth Planet. Interiors* 105 (1/2), 21–31.
- Jeanloz, R., Hemley, R.J., 1994. Thermoelasticity of perovskite: an emerging consensus. *EOS, Trans., Am. Geophys. Union* 75 (41), 476–477.
- Jeanloz, R., Kavner, A., 1996. Melting criteria and imaging spectroradiometry in laser-heated diamond-cell experiments. *Philos. Trans. R. Soc. London, Ser. A (Math. Phys. Sci.)* 354, 1279–1305.
- Jeanloz, R., Thompson, A.B., 1983. Phase transitions and mantle discontinuities. *Rev. Geophys. Space Phys.* 21 (1), 51–74.
- Knittle, E., Jeanloz, R., 1987. Synthesis and equation of state of  $(\text{Mg, Fe})\text{SiO}_3$  perovskite to over 100 GPa. *Science* 235 (4789), 668–670.
- Knittle, E., Jeanloz, R., 1991. Earth's core–mantle boundary: Results of experiments at high pressures and temperatures. *Science* 251 (5000), 1438–1443.
- Kubo, A., Akaogi, M., 2000. Post-garnet transitions in the system  $\text{Mg}_4\text{Si}_4\text{O}_{12}$ – $\text{Mg}_3\text{Al}_2\text{Si}_3\text{O}_{12}$  up to 28 GPa: Phase relations of garnet, ilmenite and perovskite. *Phys. Earth Planet. Interiors* 121 (1–2), 85–102.
- Lang, A.R., 1998. From Borrmann to super-Borrmann effect: from 2-beam to n-beam diffraction. *Cryst. Res. Technol.* 33 (4), 613–623.
- Larson, A.C., Von Dreele, R.B., 2000. Los Alamos National Laboratory Report No. LAUR 86-748 LANL.
- Lee, K.K.M., et al., 2003. Equations of state of the high-pressure phases of a natural peridotite: Implications for the Earth's lower mantle, *Earth Planet. Sci. Lett.*, submitted.
- Mao, H.K., Bell, P.M., Shaner, J.W., Steinberg, D.J., 1978. Specific volume measurements of Cu, Mo, Pd, and Ag and calibration of the ruby R1 fluorescence pressure gauge from 0.06 to 1 Mbar. *J. Appl. Phys.* 49 (6), 3276–3283.
- Navrotsky, A., et al., 2002. Aluminum in magnesian silicate perovskite: synthesis and energetics of defect solid solutions. In: Poeppelmeier, K., Navrotsky, A., Wentzcovitch, R.M. (Eds.), *Perovskite Materials*. Presented at Materials Research Society Symposium. Materials Research Society, Warrendale, PA, pp. 103–108.
- Nguyen, J.H., Jeanloz, R., 1993. A computer program to analyze X-ray diffraction films. *Rev. Sci. Instrum.* 64, 3456–3461.
- O'Neill, B., 1994. Experimental petrology of the lower mantle. PhD thesis. University of California, Berkeley, Berkeley, p. 135.
- O'Neill, B., Jeanloz, R., 1990. Experimental petrology of the lower mantle: A natural peridotite taken to 54 GPa. *Geophys. Res. Lett.* 17 (10), 1477–1480.
- O'Neill, B., Jeanloz, R., 1994.  $\text{MgSiO}_3$ – $\text{FeSiO}_3$ – $\text{Al}_2\text{O}_3$  in the Earth's lower mantle: Perovskite and garnet at 1200 km depth. *J. Geophys. Res.* 99 (B10), 19901–19915.
- Pingitore Jr., N.E., Donovan, J.J., Jeanloz, R., 1999. Electron microprobe quantification: A new model based on electrons rather than on mass. *J. Appl. Phys.* 86 (5), 2790–2794.
- Ringwood, A.E., 1975. *Composition and Petrology of the Earth's Mantle*. McGraw-Hill, New York, p. 618.
- Shim, S.H., Duffy, T.S., Kenichi, T., 2002. Equation of state of gold and its application to the phase boundaries near 660 km depth in the Earth's mantle. *Earth Planet. Sci. Lett.* 203 (2), 729–739.
- Stern, C.R., Saul, S.L., Skewes, M.A., Futa, K., 1986. Garnet peridotite xenoliths from the Pali-Aike alkali basalts of southernmost South America. In: Ross, J. (Ed.), *Proceedings of the Fourth International Kimberlite Conference. Kimberlites and Related Rocks*. Blackwell Scientific, Perth, Australia, pp. 735–744.
- Takafuji, N., Yagi, T., Miyajima, N., Sumita, T., 2002. Study on  $\text{Al}_2\text{O}_3$  content and phase stability of aluminous- $\text{CaSiO}_3$  perovskite at high pressure and temperature. *Phys. Chem. Miner.* 29, 532–537.
- Toby, B.H., 2001. EXPGUI, a graphical user interface for GSAS. *J. Appl. Crystallogr.* 34, 210–213.
- Yagi, T., Mao, H.K., Bell, P.M., 1979. Lattice parameters and specific volume for the perovskite phase of orthopyroxene composition,  $(\text{Mg, Fe})\text{SiO}_3$ . *Carnegie Inst. Washington Year Book* 78 (1790), 612–613.